RSC Advances

PAPER

View Article Online
View Journal | View Issue

Open Access Article. Published on 27 gennaio 2025. Downloaded on 02/09/2025 18:21:48.
This article is licensed under a Creative Commons Attribution-NonCommercial 3.0 Unported Licence.

Check for updates

Cite this: *RSC Adv.*, 2025, **15**, 2792

Novel magnetic nanocomposite Fe_3O_4@CS@PHMG as an effective and recyclable antimicrobial material for hospital wastewater disinfection

Lan T. Pham,[a] Hanh T. M. Le,[a] Le T. T. Tam,[ab] Hien T. Dao,[c] Minh X. Vu,[a] Thu H. A. Ngo,[d] Le T. Lu*[a] and Dung T. Nguyen*[a]

Received 10th October 2024
Accepted 6th January 2025

DOI: 10.1039/d4ra07269c

rsc.li/rsc-advances

Hospital wastewater (HWW) is a major pollutant that presents significant risks to both environmental and human health. In this study, we developed a novel, inexpensive and highly antibacterial magnetic nanocomposite composed of Fe_3O_4 nanoparticles synthesised from spent pickling liquors, coated with chitosan and then integrated with polyhexamethylene guanidine hydrochloride (Fe_3O_4@CS@PHMG) using sodium tripolyphosphate (TPP) as a crosslinking agent. The obtained results revealed that the synthesised nanocomposite exhibited high antibacterial activity against *E. coli* and *S. aureus*. At a relatively low nanocomposite dosage of 2 μg mL^{-1}, it effectively eliminated all *E. coli* at a concentration of ~10^5 CFU mL^{-1} within one min. For *S. aureus*, a higher dosage of 5 μg mL^{-1} and a longer time of 5 min were required for complete elimination. In real HWW treatment tests, 99.4% of *E. coli* and 95.8% of total coliforms were eliminated at a nanocomposite dosage of 10 μg mL^{-1}. At 30 μg mL^{-1}, the nanocomposite completely removed all *E. coli*.

Introduction

Hospital wastewater (HWW) is often considered to have pollution characteristics similar to those of domestic wastewater (DWW), leading to its collection into municipal sewage and treatment with other urban effluents. This consideration is misleading, and in reality, HWW is significantly more hazardous than DWW to both environmental and human health, as it can be a source of infectious disease transmission within communities.[1–3] Therefore, HWW requires a dedicated pretreatment before being discharged into municipal sewage. Typically, the pretreatment process of HWW is divided into 3 stages: [4] (i) primary treatments aim to remove most of the floating and heavy impurities; however, some pathogens would still be growing in this stage. (ii) Secondary treatments involve biological processes and are designed to remove most of the biodegradable organic matter and suspended solids. (iii) The final polishing treatments are disinfection processes that focus on destroying and removing most of the microbial pathogens. Thus far, chlorination remains the most commonly used disinfection method in the final step of HWW treatment owing to its high effectiveness, ease of use and low cost. However, chlorine has limited antiviral properties and can produce highly toxic by-products when it reacts with other organic substances present in wastewater.[5–7] Therefore, developing new, effective and safe disinfectants is crucial.

Numerous studies have identified effective antimicrobial polymers that exhibit low toxicity to human health.[8] Amongst these, guanidine-based polymers have garnered significant attention owing to their high antibacterial activity against a wide range of microorganisms. These polymers also possess favorable properties, such as good thermal stability, low corrosion aggressiveness, and, especially, low toxicity.[9–11] More recently, various natural polysaccharides, especially chitosan, have been extensively investigated for many biomedical applications.[11–13] However, chitosan has moderate antibacterial activity, so it is often incorporated with other antibacterial materials, such as essential oils[14–16] and silver nanoparticles.[17,18]

To enhance antibacterial efficiency and recovery ability, polymer disinfectants are often incorporated into different carriers. Amongst these, magnetic nanoparticles (MNPs) have recently emerged as a promising candidate owing to their high biocompatibility, low toxicity, and ease of separation from solution after the treatment process.[19] However, MNPs tend to aggregate with the loss of their dispersibility, and they can be stabilized by different surfactants or polymers. Chitosan is also widely used as an attractive stabilizing agent for MNPs in various interesting biomedical and environmental applications.[20–22]

[a]Institute for Tropical Technology-Vietnam Academy of Science and Technology (VAST), 18 Hoang Quoc Viet, Hanoi, Vietnam. E-mail: ndung@itt.vast.vn; ltlu@itt.vast.vn
[b]Graduate University of Science and Technology, VAST, 18 Hoang Quoc Viet, Hanoi, Vietnam
[c]Institute of Science and Technology for Energy and Environment, VAST, 18 Hoang Quoc Viet, Hanoi, Vietnam
[d]Faculty of Chemistry, University of Science, Vietnam National University, 334, Nguyen Trai, Hanoi, Vietnam

© 2025 The Author(s). Published by the Royal Society of Chemistry

Open Access Article. Published on 27 gennaio 2025. Downloaded on 02/09/2025 18:21:48.
This article is licensed under a Creative Commons Attribution-NonCommercial 3.0 Unported Licence.

To our knowledge, very few studies have explored magnetic nanocomposites with polyguanidines even though they have excellent antibacterial properties. This lack of work is likely attributable to their strong water solubility which hinders their stability in aqueous media. In our previous works, we successfully developed magnetic Fe_3O_4/polyguanidine nanocomposites and evaluated their antimicrobial ability.[23,24] In those works, the magnetic iron oxide nanoparticles were synthesised from the spent pickling liquors of a steel factory and subsequently modified with polyhexamethylene guanidine hydrochloride (PHMG). Although the as-prepared Fe_3O_4/PHMG nanocomposites exhibited excellent antimicrobial activity and could be easily separated from solution by an external magnetic field, their reusability was limited, as their antimicrobial ability decreased rapidly due to the high solubility of PHMG in water. After only a short period of immersion in water, the content of PHMG on the nanocomposite's surface decreased, resulting in a significant reduction in antibacterial activity.

In this study, we report a simple synthesis of a novel magnetic nanocomposite with enhanced antibacterial activity and reusability. Fe_3O_4 nanoparticles are synthesised from spent pickling liquors and are then coated with chitosan and further incorporated with PHMG. To prevent the release of PHMG from the nanocomposite into the solution, sodium tripolyphosphate (TPP) was used as a crosslinking agent. TPP is a polyanion that can interact with CS and PHMG through ionic interactions. This ionic crosslinking leads to the formation of a network structure, enhancing the mechanical strength and stability of the nanocomposite. The structural characteristics and antibacterial properties of the as-prepared nanocomposites were investigated; their ability to disinfect real HWW samples was also evaluated.

Experimental

Materials

Spent pickling liquors (total iron ~150 g L^{-1}, pH ~ 0.1) were collected from Hoa Phat Steel Factory (Vietnam). Chitosan (CS) with a degree of deacetylation of 96.27% and a viscosity of 294.60 cP s was supplied by Vietnam Food Joint Stock Company. Polyhexamethylene guanidine hydrochloride (PHMG) was ordered from FitoLine Co., Russia. Sodium tripolyphosphate (TPP), of reagent grade, was received from Xilong Scientific Co. (China). All chemicals were used as received without any further purification.

Synthesis of Fe_3O_4@CS@PHMG nanocomposite

Fe_3O_4 nanoparticles were synthesised using following our previous works.[23,24] In a typical process, 4.5 mL of spent pickling liquors (SPL) was added dropwise into a beaker containing 600 mL of saturated $Ca(OH)_2$ solution at room temperature (~25 °C). The solution was stirred vigorously in the air for about 45 min; pH of the mixture was about 8.0. The black precipitate of the Fe_3O_4 was separated by an external magnet. The collected Fe_3O_4 NPs, after being washed several times with distilled water, were added into 100 mL of 1.0 wt% acetic acid solution containing 0.5% CS. The mixture was stirred for 30 min to form a well-dispersed suspension of Fe_3O_4@CS NPs. The sample was then collected utilising a magnet and rinsed with distilled water to eliminate any unabsorbed CS.

For further surface modification with PHMG, a certain amount of Fe_3O_4@CS NPs was added into 100 mL of a 0.5 wt% PHMG aqueous solution, the mixture was stirred for 15 min to form a homogenous dispersion, and then 0.1 mol L^{-1} TPP solution with different volumes was added dropwise to this mixture; the weight ratios of TPP to PHMG were 5, 10, and 15%. It is important that the crosslinking agent TPP should be added dropwise into the already dispersed mixture, allowing the phosphoric ions of TPP to simultaneously react with the NH_2 groups of both CS and PHMG. As a result, the PHMG coating on CS was retained after synthesis, leading to an increase in the nanocomposite's stability.

The grafting reaction was allowed to proceed at room temperature for 4 h under continuous stirring. The resulting Fe_3O_4@CS@PHMG nanocomposites were collected using a magnet and rinsed with ethanol and distilled water before being dried at 60 °C in a vacuum oven overnight. The procedure to prepare Fe_3O_4@CS@PHMG nanocomposite is presented in Fig. 1.

Characterisation

Thermogravimetric analysis (TGA) was performed with a NETZSCH TG 209 F1 Libra instrument from room temperature to 600 °C in air at heating rate of 10 °C min^{-1}. The magnetic properties of the samples were studied using a vibrating sample magnetometer (VSM, DMS 800, Quantum Design, Inc.). The saturation magnetization (M_s) and coercive field (H_c) were measured at room temperature with the magnetic field ranging from −10 to 10 kOe. X-ray diffraction (XRD) analysis was carried out on a Siemens/Bruker D5005 diffractometer using Cu Kα radiation ($\lambda = 0.154$ nm). The data were collected over a range from 10° to 70°, with a step size of 0.03°. Fourier transform infrared (FT-IR) spectra were recorded on a Thermo Scientific Nicolet iS10 FT-IR Spectrometer with diamond ATR. For the morphology characterization, we used a transmission electron microscope (JEOL JEM-1010, Peabody, MA, USA) operated at 80 kV.

Antibacterial tests

The antibacterial properties of the Fe_3O_4@CS@PHMG nanocomposites against *Escherichia coli* (Gram negative) and *Staphylococcus aureus* (Gram positive) were evaluated. Initially, 2 mL of a bacterial suspension (~10^7 CFU mL^{-1}) was added to 198 mL of solution containing Fe_3O_4@CS@PHMG at varying dosages, from 0.25 to 5 μg mL^{-1}. The flask was shaken at 500 rpm, and after different time intervals, 0.2 mL of the solution was plated onto solid agar Petri dishes (using Plate Count Agar) and spread evenly. All plates were incubated at 37 °C for 24 h, after which the colonies formed were counted manually. Each sample was tested in triplicate. The antimicrobial activity was quantified as the percentage reduction of bacterial growth after exposure to

Open Access Article. Published on 27 gennaio 2025. Downloaded on 02/09/2025 18:21:48.
This article is licensed under a Creative Commons Attribution-NonCommercial 3.0 Unported Licence.

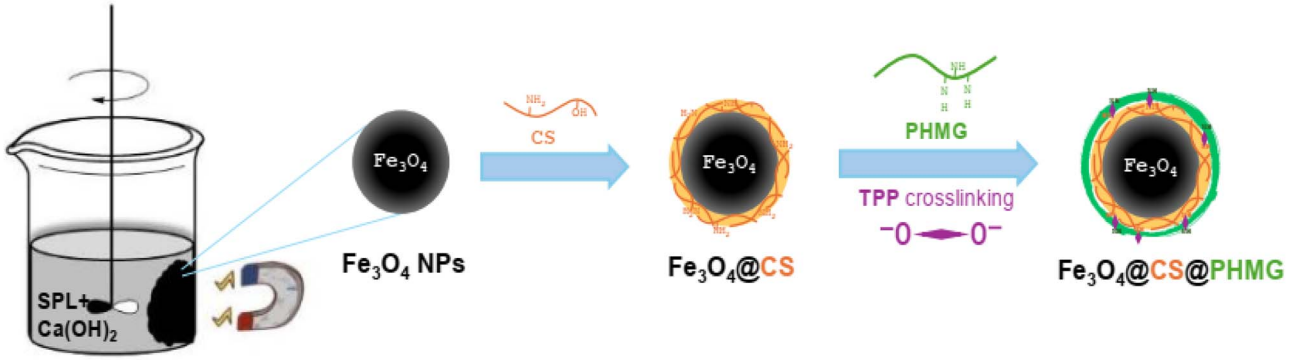

Fig. 1 Schematic of the preparation of Fe_3O_4@CS@PHMG nanocomposite.

the nanocomposite solution, calculated using the following equation,

$$H(\%) = \left(1 - \frac{N}{A}\right) \times 100\%$$

where A is the number of bacterial colonies in the untreated suspension (without nanocomposite) and N is the number of bacterial colonies in the treated suspension (in the presence of nanocomposite).

The reusability of the nanocomposite was tested using the same procedure. After 1 min of exposure to the bacterial suspension, the sample was collected with a magnet and reused for further repeated tests 4 more times.

Disinfection of hospital wastewater sample

The HWW samples were collected from National Traditional Medicine Hospital (Hanoi, Vietnam), after preliminary treatment and secondary biological treatment processes. The main characteristics of the sewage and sample treated using Fe_3O_4@CS@PHMG nanocomposites, including pH, turbidity, COD, *E. coli*, and total coliform, were determined following standard methods for the examination of water and wastewater (ISO 10523:2008, ISO 7027-1:2016, SMEWW 5220C:2012, ISO 9308-1:2014).

Results and discussion

Characterisation of the Fe_3O_4@CS@PHMG nanocomposite

TGA analysis. Thermogravimetric curves of Fe_3O_4 NPs, Fe_3O_4@CS, and Fe_3O_4@CS@PHMG nanocomposites synthesised with different ratios of crosslinking agent TPP are presented in Fig. 2. As can be seen, Fe_3O_4 NPs exhibit very good thermal stability up to 600 °C with negligible weight loss in the TGA curve (curve a). The TGA curve of Fe_3O_4@CS NPs shows a weight loss of about 2% starting from approximately 200 to 380 °C (curve b) related to the decomposition of CS. For the Fe_3O_4@CS@PHMG nanocomposites, the resulting TGA curves (curves c–f) clearly exhibit the influence of the TPP ratios on the amount of PHMG incorporated into Fe_3O_4@CS NPs. The weight loss of Fe_3O_4@CS@PHMG increases with higher TPP ratios; the amounts of PHMG were determined to be approximately 2, 8 and 14% for the TPP ratios of 5, 10, and 15%, respectively. In the absence of TPP (curve c), only a small amount of PHMG is physically adsorbed onto the Fe_3O_4@CS NPs.

Magnetic property. The magnetisation hysteresis curves of Fe_3O_4 NPs and Fe_3O_4@CS@PHMG nanocomposite samples were obtained using VSM magnetometry under a magnetic field ranging from −10 to 10 kOe at room temperature, as shown in Fig. 3. These curves indicate the high saturation magnetisation for both the pure and composite nanoparticles; the samples are superparamagnetic as no coercivity or remanence is observed. As can be seen, Fe_3O_4 NPs synthesised from SPL exhibit a very high saturation magnetisation value (M_s) of 73.8 emu g^{-1}. In contrast, the M_s values of the Fe_3O_4@CS@PHMG nanocomposites decrease as the PHMG content increases (with increasing TPP ratio). The nanocomposite sample with a TPP to PHMG ratio of 10% was chosen for further investigation due to its high M_s value of 59.5 emu g^{-1} which allows it to be easily separated from wastewater after treatment.

XRD analysis. As shown in Fig. 4, the structural phase of Fe_3O_4 prepared using the SPL precursor reflected at 2θ angles of 30.15°, 35.56°, 43.27°, 53.58°, 57.35° and 62.82°, corresponding

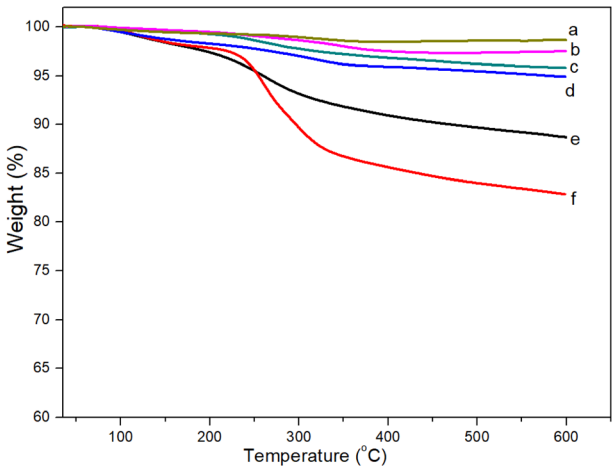

Fig. 2 TGA curves of Fe_3O_4 NPs (a) Fe_3O_4@CS (b) and Fe_3O_4@CS@PHMG nanocomposites with different weight ratios of TPP: 0 (c), 5 (d), 10 (e) and 15% (f).

 © 2025 The Author(s). Published by the Royal Society of Chemistry

Open Access Article. Published on 27 gennaio 2025. Downloaded on 02/09/2025 18:21:48.
This article is licensed under a Creative Commons Attribution-NonCommercial 3.0 Unported Licence.

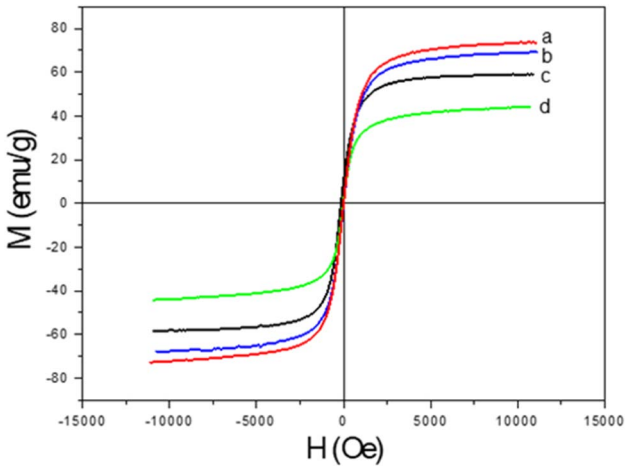

Fig. 3 Magnetisation curves of Fe_3O_4 NPs (a) and Fe_3O_4@CS@PHMG nanocomposites with different TPP ratios of 5 (b), 10 (c), and 15% (d).

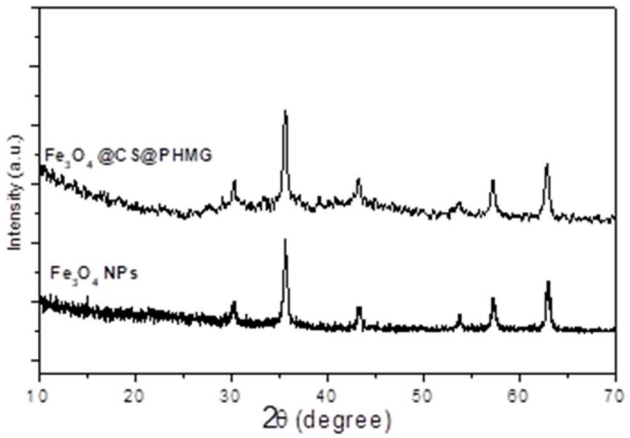

Fig. 4 XRD patterns of Fe_3O_4 and Fe_3O_4/@CS@PHMG nanocomposite.

to the (220), (311), (400), (422), (511) and (440) crystal planes of Fe_3O_4 NPs.[25] The absence of the characteristic diffraction peaks at (113), (210) and (213) of maghemite and hematite[26] indicates that the nanoparticles synthesized from SPL in our work are single phase. The diffraction peaks of Fe_3O_4/@CS@PHMG nanocomposite did not change.

FT-IR analysis. The chemical structure of the Fe_3O_4@CS@PHMG nanocomposite (prepared at 10% TPP) was characterised by FT-IR spectroscopy. Sole Fe_3O_4, CS and PHMG samples were also recorded for comparison (Fig. 5).

As illustrated in Fig. 5, the FT-IR spectrum of the Fe_3O_4@CS@PHMG nanocomposite (Fig. 5D) shows the presence of all three components, with the band at the wavenumber of 574 cm^{-1} corresponding to Fe–O stretching vibrations.[27] The band at 1635 cm^{-1}, attributed to the bending vibrations of the –OH groups on the surface of Fe_3O_4 NPs, could overlap with the band of C=N stretching vibrations of PHMG at 1636 cm^{-1}.[9,28]

The characteristic absorption peaks of CS can also be seen: the peak at 1528 cm^{-1} is attributed to N–H groups, the

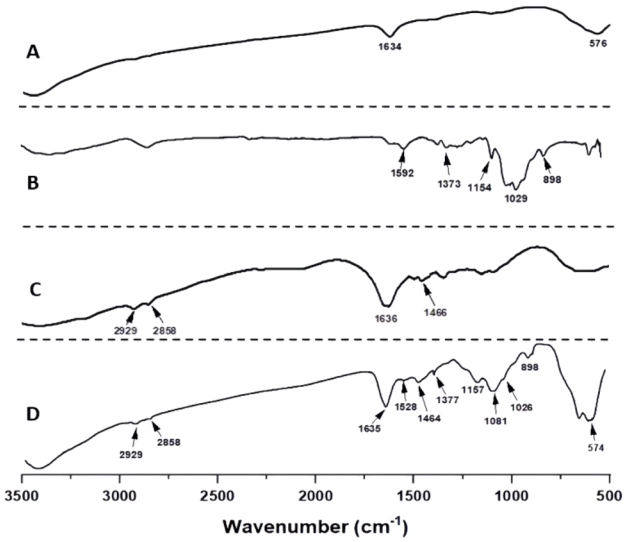

Fig. 5 FT-IR spectra of Fe_3O_4 (A), chitosan (B), PHMG (C) and Fe_3O_4@CS@PHMG samples (D).

absorption bands at 1377 and 1157 cm^{-1} are attributed to the asymmetric stretching of the C–O–C bridge, the peak at 898 cm^{-1} corresponds to the CH bending out of the plane of the ring in monosaccharides, and the peak at 1026 cm^{-1} corresponds to C–O stretching.[29] The characteristic bands of PHMG are observed, appearing at 2929 and 2850 cm^{-1}, and are assigned respectively to the asymmetric and symmetric stretching vibrations of the CH_2 groups; the peak at 1464 cm^{-1} is related to the bending vibrations of the amine group.[9,26] Moreover, as observed in Fig. 5D, the absorption peak of the P=O group appears at 1081 cm^{-1},[30] indicating the presence of the crosslinking agent TPP in the nanocomposite composition.

TEM analysis. Fig. 6 shows the TEM images of Fe_3O_4 NPs and the Fe_3O_4@CS@PHMG nanocomposite. It can be seen that the MNPs maintain their spherical shape after modification with CS and PHMG; however, the size of the composite particles (20–35 nm) is slightly larger than that of the Fe_3O_4 core particles (10–25 nm).

Antibacterial activity

In this work, the antibacterial activity of the Fe_3O_4@CS@PHMG nanocomposite was tested against *E. coli* (3.1×10^5 CFU mL^{-1}) and *S. aureus* (2.8×10^5 CFU mL^{-1}). Fig. 7 demonstrates the antibacterial efficiency against these bacteria at different contact times using varying amounts of the Fe_3O_4@CS@PHMG nanocomposites. The photographs of some samples for bacterial concentration determination are shown in Fig. 8.

As can be seen, Fe_3O_4@CS@PHMG nanocomposites exhibit strong and fast-acting bactericidal activity. In all cases studied, they demonstrate their antibacterial effect in less than 5 min. The Fe_3O_4@CS@PHMG nanocomposite at a dose of 2 μg mL^{-1} can eliminate all *E. coli* in the solution within only 1 min, and it requires a dose of 5 μg mL^{-1} for *S. aureus*. It has been previously reported that pure PHMG is more effective against *E. coli* than against *S. aureus*.[9,10,31]

Open Access Article. Published on 27 gennaio 2025. Downloaded on 02/09/2025 18:21:48.
This article is licensed under a Creative Commons Attribution-NonCommercial 3.0 Unported Licence.

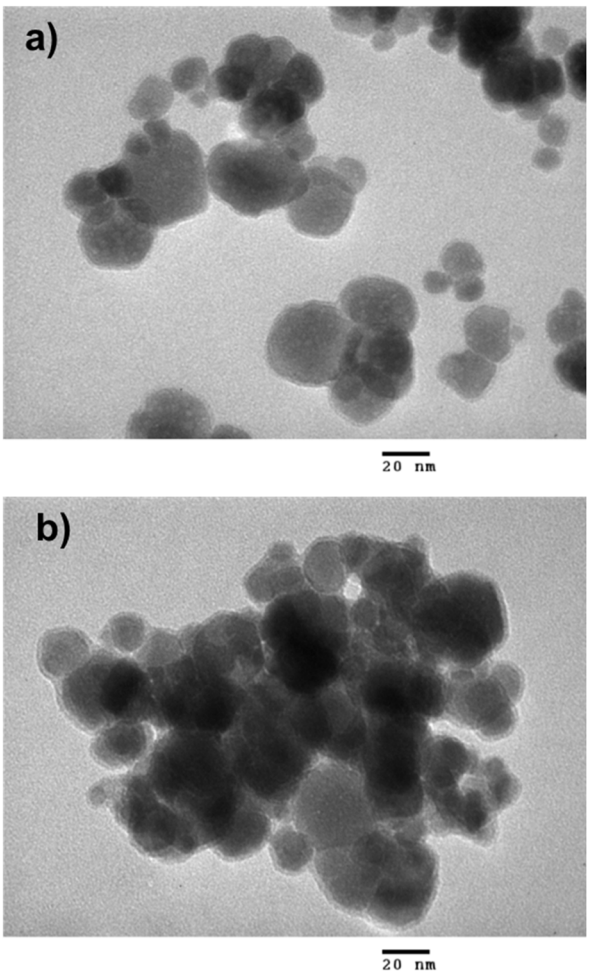

Fig. 6 TEM images of Fe_3O_4 (a) and Fe_3O_4@CS@PHMG nanocomposites (b).

In comparison to a similar material, polyethylene glycol and polyhexamethylene guanidine hydrochloride dual-polymer-functionalized graphene oxide (GO-PEG-PHMG), that can eliminate *E. coli* and *S. aureus* with density of 10^4 CFU mL^{-1} at a dose of 4 mg mL^{-1} after 30 min of contact,[32] the antibacterial effect of Fe_3O_4@CS@PHMG nanocomposites is clearly much higher.

Fe_3O_4 and Fe_3O_4@CS NPs were also tested in the same conditions, but they showed no antibacterial efficiency, even at higher dosage (up to 1 mg mL^{-1}) and with longer contact time (up to 4 hours). This is because of the moderate antibacterial activity of both Fe_3O_4 NPs and CS.[33,34] Fe_3O_4@CS@PHMG nanocomposites have much higher antibacterial activity because of strong biocidal action of covered PHMG. PHMG can be also released from the nanocomposite, therefore increasing the interaction between biocide and bacteria in the solution.

It is widely known that magnetic Fe_3O_4 NPs have insignificant antimicrobial activity,[33,34] and, in this study, NPs are primarily used for reuse *via* magnetic separation after the disinfection process. Additionally, CS has moderate antibacterial activity, and the contact between Fe_3O_4@CS NPs and the bacteria in the solution was quite limited, so they did not show antibacterial effects. PHMG is an excellent biocide that can destroy bacteria initially through strong electrostatic interactions with the negatively charged bacterial cell surface, leading to the leakage of cell contents and cytosol coagulation.[10,11] During the antibacterial test in this study, the flask containing Fe_3O_4@CS@PHMG nanocomposites was shaken, which may have resulted in the release of PHMG into the solution. This is because the CS-TPP-PHMG linkage was not strong enough, allowing PHMG to rapidly interact with and destroy all the bacteria in the solution.

Reusability evaluation

The reusability of the Fe_3O_4@CS@PHMG nanocomposites was tested for *E. coli* treatment under the following conditions: disinfectant concentration of 2 μg mL^{-1}, *E. coli* concentration of 7.7×10^5 CFU mL^{-1} and a contact time of 1 min. After the first treatment, Fe_3O_4@CS@PHMG nanocomposites were separated by a magnet and continued to be used for a further 4 times. The

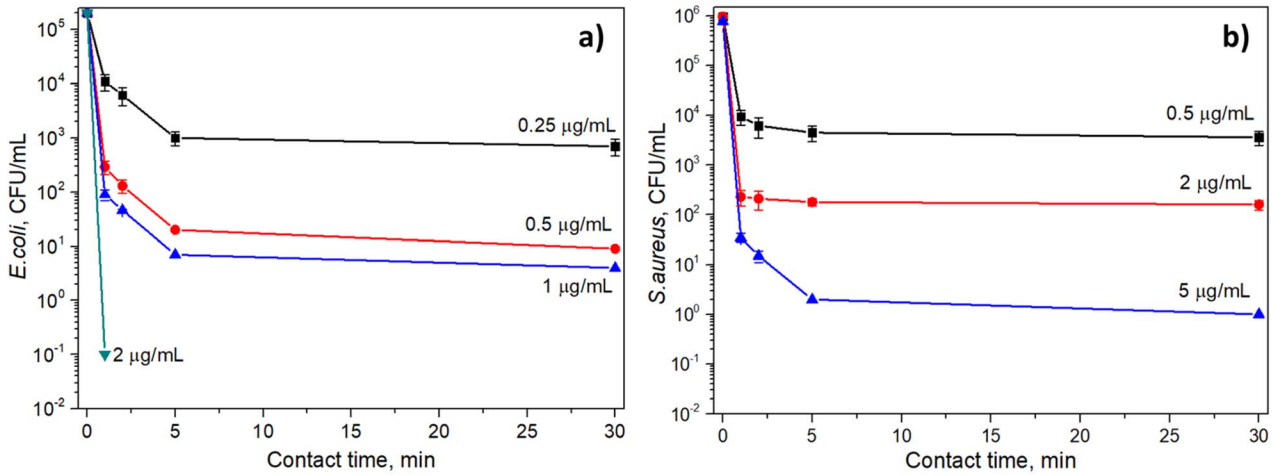

Fig. 7 Antibacterial efficiency at different contact times and Fe_3O_4@CS@PHMG nanocomposite dosages against *E. coli* (a) and *S. aureus* (b).

 © 2025 The Author(s). Published by the Royal Society of Chemistry

Open Access Article. Published on 27 gennaio 2025. Downloaded on 02/09/2025 18:21:48.
This article is licensed under a Creative Commons Attribution-NonCommercial 3.0 Unported Licence.

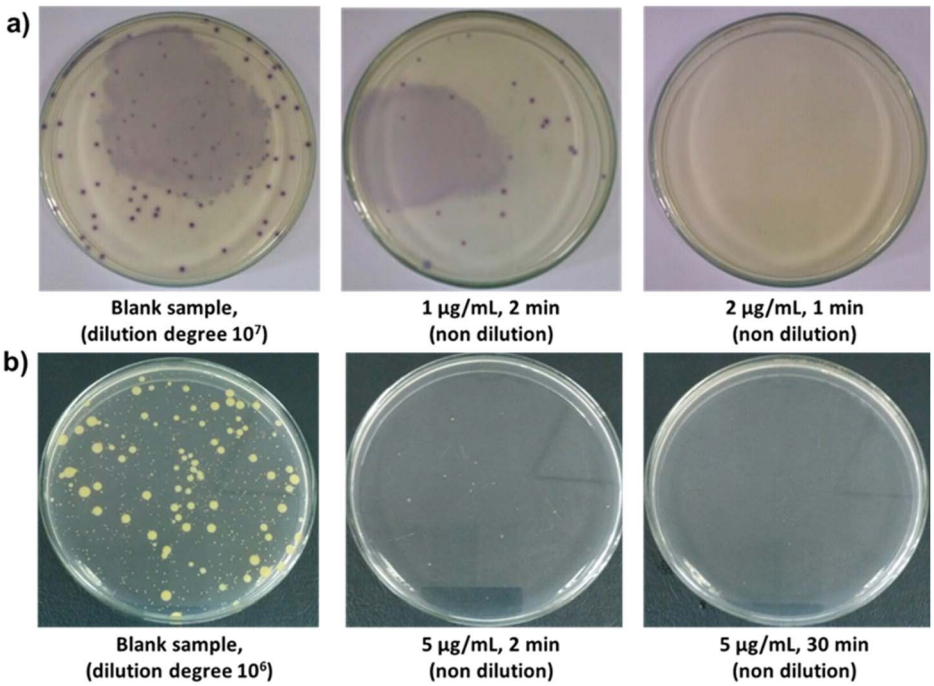

Fig. 8 Photographs of *E. coli* (a) and *S. aureus* (b) grown on LB agar plates after treatment with different dosages of Fe_3O_4@CS@PHMG and different contact times.

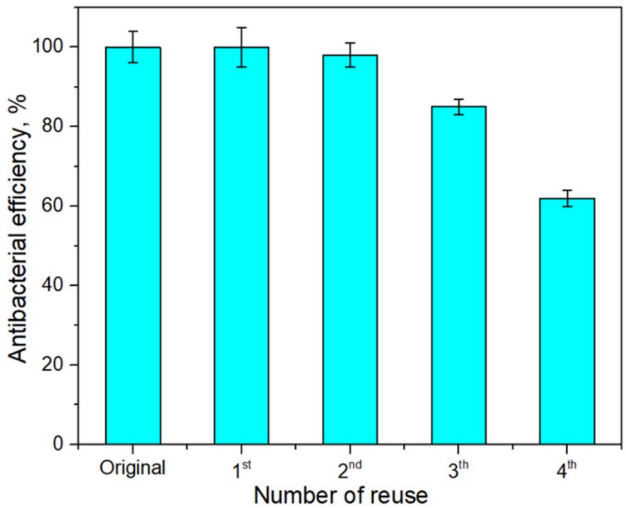

Fig. 9 Antibacterial efficiency of the Fe_3O_4@CS@PHMG (2 μg mL^{-1}) against *E. coli* (7.7 × 10^5 CFU mL^{-1}) after several reuse cycles.

antibacterial efficiencies were determined and are presented in Fig. 9.

As shown in Fig. 9, the Fe_3O_4@CS@PHMG nanocomposites retained an antibacterial efficiency of almost 100% for the first three uses, after which their activity began to decline, and it was about 62% for the fourth use. In contrast, the Fe_3O_4@PHMG nanocomposites without crosslinking exhibit their high antibacterial efficiency only during the first use with negligible efficiency remaining in the subsequent uses (data not shown). The reduction in the antibacterial activity of the Fe_3O_4@CS@PHMG nanocomposites is possibly due to the release of the biocidal PHMG from the nanocomposites after four cycles during vigorous mixing (500 rpm).

Disinfection of the real HWW samples

The wastewater samples used in this work were taken from National Traditional Medicine Hospital (Hanoi, Vietnam) after the primary and secondary biological treatment processes. The main parameters of these samples are summarized in Table 1. The HWW samples collected after treatment in the bioreactor still contain numerous microorganisms with the densities of *E. coli* and total coliforms being significantly higher than the recommended concentrations according to the Ministry of Health's domestic water quality standards (QCVN 02:2009/BYT).

The sewage samples were treated using sole PHMG (at a dose of 10 μg mL^{-1}) and Fe_3O_4@CS@PHMG nanocomposites (at two dosages of 10 and 30 μg mL^{-1}) with a contact time of 30 min. Herein, a dosage of 10 μg mL^{-1} of sole PHMG was chosen according to ref. 35, which indicated that PHMG completely inhibited both Gram-positive and Gram-negative bacteria cultured in the laboratory at a density of 10^6 CFU mL^{-1}.

As shown in Table 1, the treatment process resulted in a slight reduction in the turbidity of the HWW sample, but pH and COD values remained similar to the values of the sample pre-treatment. This indicates that neither PHMG nor Fe_3O_4@CS@PHMG nanocomposite effectively removes trace organics. However, both treatments effectively eliminate pathogens in the HWW samples at low dosages. The Fe_3O_4@CS@PHMG nanocomposite removed over 99.4% of *E. coli* and 95.8% of total coliforms at a dosage of 10 μg mL^{-1}. These results are significantly lower than the antibacterial efficiencies observed for the

Open Access Article. Published on 27 gennaio 2025. Downloaded on 02/09/2025 18:21:48.
This article is licensed under a Creative Commons Attribution-NonCommercial 3.0 Unported Licence.

Table 1 Characteristics of HWW sample before and after treatment by pristine PHMG and Fe_3O_4@CS@PHMG nanocomposite

		After treatment			Standard QCVN 02:2009/BYT	
Parameter (unit)	Sewage	PHMG (10 μg mL^{-1})	Fe_3O_4@CS@PHMG (10 μg mL^{-1})	Fe_3O_4@CS@PHMG (30 μg mL^{-1})	Class 1	Class 2
pH	7.2	7.1	7.2	7.3	6.0–8.5	6.0–8.5
Turbidity (NTU)	15	5	8	5	5	5
COD (mg L^{-1})	63	65	62	60	—	—
E. coli (CFU/100 mL)	8×10^3	0 ($H = 100\%$)	50 ($H = 99.4\%$)	0 ($H = 100\%$)	0	20
Total coliforms (CFU/100 mL)	1.3×10^4	50 ($H = 99.4\%$)	540 ($H = 95.8\%$)	100 ($H = 99.2\%$)	50	150

lab-cultivated bacteria (Section 3.2), possibly due to a higher antibiotic resistance of bacteria in the real HWW samples.

In comparison with sole PHMG, the Fe_3O_4@CS@PHMG nanocomposite exhibited a slightly lower antibacterial efficiency (Table 1). This is due to a smaller amount of PHMG in the nanocomposite composition (∼14%). However, at a dosage of 30 μg mL^{-1}, the nanocomposite successfully eliminated all *E. coli* in the HWW sample, and the total coliform count was reduced to below the recommended limit according to class 2 of the QCVN 02:2009/BYT standard.

Conclusions

In this study, the synthesis of novel magnetic antibacterial Fe_3O_4@CS@PHMG nanocomposite was performed using by-products of steel and food factories (spent pickling liquors and chitosan). Characterization studies, including TGA, VSM, FT-IR and TEM analysis, demonstrated the successful integration of PHMG into the Fe_3O_4@CS matrix through chemical bonding with sodium tripolyphosphate. The synthesis of the nanocomposite is relatively simple and scalable, and the obtained Fe_3O_4@CS@PHMG exhibits strong antibacterial properties against both *E. coli* and *S. aureus*, with rapid and effective action at low concentrations. Furthermore, the as-prepared nanocomposite demonstrated improved washing resistance and can be reused several times with enhanced recovery capability *via* external magnetic field. We also demonstrate that the nanocomposite effectively disinfected real HWW samples, significantly reducing the levels of *E. coli* and total coliforms, meeting the recommended limits according to the QCVN 02:2009/BYT standard. We are confident that this material has strong potential for practical applications, especially if an effective system for recovering and reusing the nanocomposite can be developed.

Data availability

All data supporting the findings of this study are included within the manuscript.

Author contributions

Lan T. Pham and Dung T. Nguyen conceptualized the study and designed the methodology. Hanh T. M. Le, Le T. T. Tam, Hien T. Dao, Minh X. Vu, and Thu H. A. Ngo conducted the experiments, collected, and analyzed the data. Le T. Lu and Dung T. Nguyen acquired funding, supervised the project, and contributed to writing and revising the manuscript. All authors reviewed and approved the final manuscript.

Conflicts of interest

The authors declare that they have no competing interests.

Acknowledgements

The authors are grateful for the financial support from the National Foundation for Science and Technology Development (NAFOSTED) under Grant No. 104.02-2019.331.

References

1 P. Verlicchi, A. Galletti and L. Masotti, *Water Sci. Technol.*, 2010, **61**, 2507–2519.
2 F. Saguti, E. Magnil, L. Enache, M. P. Churqui, A. Johansson, D. Lumley, F. Davidsson, L. Dotevall, A. Mattsson, E. Trybala, M. Lagging, M. Lindh, M. Gisslén, T. Brezicka, K. Nyström and H. Norder, *Water Res.*, 2021, **189**, 116620.
3 T. Yuan and Y. Pia, *Front. Environ. Sci.*, 2023, **10**, 1734.
4 P. Verlicchi, M. Al Aukidy and E. Zambello, *Sci. Total Environ.*, 2015, **514**, 467–491.
5 E. Emmanuel, G. Keck, J. M. Blanchard, P. Vermande and Y. Perrodin, *Environ. Int.*, 2004, **30**, 891–900.
6 M. N. Wu, X. C. Wang and X. Y. Ma, *J. Hazard. Mater.*, 2013, **261**, 325–331.
7 S. Sorlini, M. Biasibetti, F. Gialdini and M. C. Collivignarelli, *Water Sci. Technol.: Water Supply*, 2016, **16**, 333–346.
8 M. R. E. Santos, A. C. Fonseca, P. V. Mendonça, R. Branco, A. C. Serra, P. V. Morais and J. F. J. Coelho, *Materials*, 2016, **9**, 599.
9 G. M. Nikolaevna, S. S. Aleksandrovich, A. S. Aleksandrovna, T. I. Mihaylovna, B. L. Ulzitovna, B. V. Babudorjievich and M. D. Markovich, *J. Appl. Polym. Sci.*, 2014, **131**, 40319.
10 M. K. Oulé, R. Azinwi, A. M. Bernier, T. Kablan, A. M. Maupertuis, S. Mauler, R. K. Nevry, K. Dembélé, L. Forbes and L. Diop, *J. Med. Microbiol.*, 2008, **57**, 1523–1528.

 © 2025 The Author(s). Published by the Royal Society of Chemistry

Open Access Article. Published on 27 gennaio 2025. Downloaded on 02/09/2025 18:21:48.
This article is licensed under a Creative Commons Attribution-NonCommercial 3.0 Unported Licence.

11 H. Choi, K.-J. Kim and D. G. Lee, *Fungal Biol.*, 2017, **121**, 53–60.
12 A. Muñoz-Bonilla, C. Echeverria, Á. Sonseca, M. P. Arrieta and M. Fernández-García, *Materials*, 2019, **12**, 641.
13 Y. N. Gavhane, A. S. Gurav and A. V. Yadav, *Int. J. Res. Pharm. Biomed. Sci.*, 2013, **4**, 312–321.
14 R. Priyadarshi, Sauraj, B. Kumar, F. Deeba, A. Kulshreshtha and Y. S. Negi, *Food Hydrocolloids*, 2018, **85**, 158–166.
15 V. L. C. D. Alves, B. P. M. Rico, R. M. S. Cruz, A. A. Vicente, I. Khmelinskii and M. C. Vieira, *LWT–Food Sci. Technol.*, 2018, **89**, 525–534.
16 K. Li, G. Guan, J. Zhu, H. Wu and Q. Sun, *Food Control*, 2019, **96**, 234–243.
17 M. A. Huq, M. Ashrafudoulla, M. A. K. Parvez, S. R. Balusamy, M. M. Rahman, J. H. Kim and S. Akter, *Polymers*, 2022, **14**, 5302.
18 P. Senthilkumar, G. Yaswant, S. Kavitha, E. Chandramohan, G. Kowsalya, R. Vijay, B. Sudhagar and D. S. R. S. Kumar, *Int. J. Biol. Macromol.*, 2019, **141**, 290–298.
19 R. D. Ambashta and M. Sillanpää, *J. Hazard. Mater.*, 2010, **180**, 38–49.
20 A. M. Grumezescu, E. Andronescu, A. M. Holban, A. Ficai, D. Ficai, G. Voicu, V. Grumezescu, P. C. Balaure and C. M. Chifiriuc, *Int. J. Pharm.*, 2013, **454**, 233–240.
21 A. Allafchian, H. Bahramian, S. A. H. Jalali and H. Ahmadvand, *J. Magn. Magn. Mater.*, 2015, **394**, 318–324.
22 K. Zomorodian, H. Veisi, S. M. Mousavi, M. S. Ataabadi, S. Yazdanpanah, J. Bagheri, A. P. Mehr, S. Hemmati and H. Veisi, *Int. J. Nanomed.*, 2018, **13**, 3965–3973.
23 D. T. Nguyen, L. T. Pham, H. T. T. Le, M. X. Vu, H. T. M. Le, H. T. M. Le, N. H. Pham and L. T. Lu, *RSC Adv.*, 2018, **8**, 19707–19712.
24 M. X. Vu, H. T. T. Le, L. T. Pham, N. H. Pham, H. T. M. Le, L. T. Le and D. T. Nguyen, *Izv. Vyssh. Uchebn. Zaved., Khim. Khim. Tekhnol.*, 2018, **61**, 59–63.
25 B. Aslibeiki, P. Kameli, I. Manouchehri and H. Salamati, *Curr. Appl. Phys.*, 2012, **12**, 812–816.
26 J. Murbe, A. Rechtenbach and J. Topfer, *Mater. Chem. Phys.*, 2008, **110**, 426–433.
27 K. Petcharoen and A. Sirivat, *Mater. Sci. Eng., B*, 2012, **177**, 421–427.
28 M. N. Grigor'eva, S. A. Stel'makh, S. A. Astakhova, I. M. Tsenter, L. U. Bazaron, V. B. Batoev and D. M. Mognonov, *J. Appl. Polym. Sci.*, 2014, **131**, 40319.
29 E. M. Dahmane, M. Taourirte, N. Eladlani and M. Rhazi, *Int. J. Polym. Anal. Charact.*, 2014, **19**, 342–351.
30 M. S. Gurses, C. Erkey, S. Kizilel and A. Uzun, *Talanta*, 2018, **176**, 8–16.
31 J. Nikkola, X. Liu, Y. Li, M. Raulio, H. L. Alakomi, J. Wei and C. Y. Tang, *J. Membr. Sci.*, 2013, **444**, 192–200.
32 P. Li, S. Sun, A. Dong, Y. Hao, S. Shi, Z. Suna, G. Gao and Y. Chen, *Appl. Surf. Sci.*, 2015, **355**, 446–452.
33 S. S. Behera, J. K. Patra, K. Pramanik, N. Panda and H. Thatoi, *World J. Nano Sci. Eng.*, 2012, **2**, 196–220.
34 U. S. Ezealigo, B. N. Ezealigo, S. O. Aisida and F. I. Ezema, *JCIS Open*, 2021, **4**, 100027.
35 D. Wei, Q. Ma, Y. Guan, F. Hu, A. Zheng, X. Zhang, Z. Teng and H. Jiang, *Mater. Sci. Eng., C*, 2009, **29**, 1776–1780.